ELSEVIER

Cold Regions Science and Technology 35 (2002) 147–167

cold regions science and technology

www.elsevier.com/locate/coldregions

A physical SNOWPACK model for the Swiss avalanche warning Part II. Snow microstructure

Michael Lehning[a,*], Perry Bartelt[a], Bob Brown[a,b], Charles Fierz[a], Pramod Satyawali[a,c]

[a] *WSL, Swiss Federal Institute for Snow and Avalanche Research SLF, Flüelastr. 11, CH-7260 Davos-Dorf, Switzerland*
[b] *Department of Civil Engineering, Montana State University, Bozeman, MT, USA*
[c] *Snow and Avalanche Study Establishment, Manali, India*

Abstract

The snow cover model SNOWPACK includes a detailed model of snow microstructure and metamorphism. In SNOWPACK, the complex texture of snow is described using the four primary microstructure parameters: grain size, bond size, dendricity and sphericity. For each parameter, rate equations are developed that predict the development in time as a function of the environmental conditions. The rate equations are based on theoretical considerations such as mixture theory and on empirical relations. With a classification scheme, the conventional snow grain types are predicted on the basis of those parameters. The approach to link the bulk constitutive properties, viscosity and thermal conductivity to microstructure parameters is novel to the field of snow cover modeling. Expanding on existing knowledge on microstructure-based viscosity and thermal conductivity, a complete description of those quantities applicable to the seasonal snow cover is presented. This includes the strong coupling between physical processes in snow: The bond size, which changes not only through metamorphic processes but also through the process of pressure sintering (included in our viscosity formulation), is at the same time the single most important parameter for snow viscosity and thermal conductivity. Laboratory results are used to illustrate the performance of the formulations presented. The numerical implementation is treated in the companion paper Part I. A more complete evaluation for the entire model is found in the companion paper Part III.

Keywords: SNOWPACK; Snow microstructure; Snow texture; Microstructure parameters; Grain size; Bond size; Dendricity; Sphericity; Snow viscosity; Thermal conductivity

1. Introduction

Snow has a complex microstructure which changes constantly as a function of the environmental conditions. The microstructure determines the bulk characteristics of the snow pack such as the temperature distribution, its settling rate and its many additional mechanical properties, e.g. shear strength and hardness. A general introduction to the snow cover model SNOWPACK is given in the companion paper Part I (Bartelt and Lehning, this issue) and a summarizing overview in Lehning et al. (1999). Meteorological boundary conditions are treated in Part III (Lehning et al., this issue) Here, we present the formulations that are used to describe snow microstructure and snow metamorphism. First, we define the four SNOWPACK microstructure parameters bond size, grain

* Corresponding author. Tel.: +41-81-417-0158; fax: +41-81-417-0110.
E-mail address: lehning@slf.ch (M. Lehning).

0165-232X/02/$ - see front matter © 2002 Elsevier Science B.V. All rights reserved.
PII: S0165-232X(02)00073-3

size, dendricity and sphericity. Second, we develop rate equations for those parameters. Third, we establish the link to the conventional grain types. Fourth, we link the parameters to the bulk constitutive properties viscosity and thermal conductivity.

We build on existing knowledge and work (Colbeck, 1987; Brun et al., 1992), and whenever appropriate, we adopt or adapt formulations presented earlier and give the corresponding reference. A general overview on snow mechanics and snow microstructure with an exhaustive reference list is in Shapiro et al. (1997). This overview and references therein describe the development of scientific knowledge on which we build. However, we also present new formulations and concepts combined with new laboratory experimental data because a consistent, detailed and complete description of microstructure, metamorphism and their macroscopic effects on the seasonal snow cover is not available at present. These new results fill important gaps in our knowledge and allow a more physical model description of processes in the seasonal snow cover. An appropriate example is the formulation for kinetic bond growth and the comparison of the model to laboratory experimental data. A further example is our approach to use the microstructure to predict bulk snow properties such as thermal conductivity and viscosity.

2. Snow microstructure

The microstructure of snow plays an extremely important role in determining the global properties of snow. This includes optical properties (albedo, extinction coefficient), mechanical properties (viscosity, Young's modulus, strength) and physical properties (thermal conductivity, diffusivity, dielectric constant). These properties vary with the density of snow, but at any given density, they can vary by as much as an order of magnitude due to differences in the material microstructure (Bartelt and von Moos, 2000). The important snow surface characteristic threshold friction velocity is also dependent on snow microstructure and crucial for a correct description of snowdrift (Lehning et al., 2000a,b).

By microstructure, we mean the geometrical shapes that define the grain size, grain shape, pore size, pore shape and the nature of the intergranular bonding. Fig. 1 shows a surface section of well-bonded rounded snow and motivates our use of

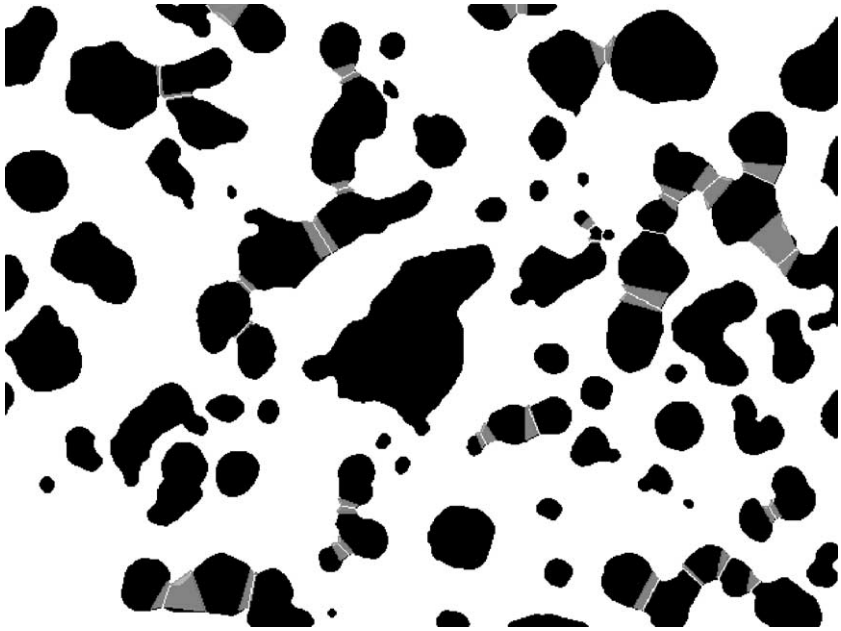

Fig. 1. Surface section image of well-bonded snow. The necks are outlined as the grey areas.

microstructure parameters to describe snow properties. An added feature of the microstructure could include the statistical distribution of these variables and their variation with orientation. This latter feature determines the isotropy of the material. Currently, SNOWPACK uses four primary, i.e. independent microstructure parameters: sphericity, dendricity (Brun et al., 1992), grain size and bond size. All other microstructure parameters of SNOWPACK can be derived from these four parameters. An additional important property is the three-dimensional coordination number, which is currently a derived parameter. This is the number of bonds per grain and determines the interconnectivity of the ice matrix.

The consideration of bond size is novel in snow pack modeling. Bond or neck size crucially influences the mechanical properties of snow. Necks are the constricted regions connecting the ice grains. The neck geometry can be defined in any of a number of ways. Fig. 2 illustrates the geometry used in this paper. The neck connects the two grains. The bond radius r_b is defined to be the minimum constriction in the neck, and the neck length l_n is the length of the neck along the neck axis as shown in the figure, i.e. the distance between the neck bases.

The neck is a critical factor in determining many of the physical and mechanical properties of snow, or for that matter, any cohesive granular material. Stresses within the material reach peak values within the necks, since they transfer all loads between the ice grains. The grains, being more massive and structurally more rigid than the necks, can transfer loads to the necks without undergoing substantial deformations. The necks, on the other hand, experience larger stresses and subsequently begin yielding and flowing much more readily than the ice grains. Triaxial tests with snow indicate that neck stresses are between 5 and 50 times higher than the grain stresses. (Bartelt and von Moos, 2000). This all depends on grain size, bond size and the three-dimensional coordination number.

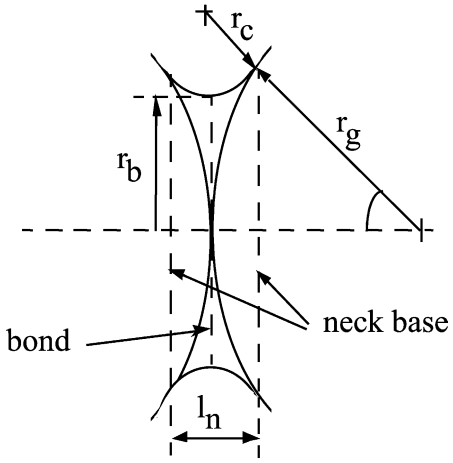

Fig. 2. Assumed model geometry for bonds and necks.

2.1. Snow metamorphism

Three types of metamorphism determine the continuous change of texture in deposited snow: equilibrium growth metamorphism, kinetic growth metamorphism and melt metamorphism. Equilibrium and kinetic growth metamorphism are governed by water vapor gradients between convex and concave surfaces and between ice matrix and pore space, respectively. Kinetic growth and wet metamorphism are very dynamic forms of metamorphism which cause rapid changes in the microstructure and material properties. We refer to the reviews by Arons and Colbeck (1995) and Colbeck (1987) for further reading.

2.1.1. Equilibrium growth metamorphism

We will name equilibrium growth metamorphism also equitemperature (ET) metamorphism and define it as the snow development under small temperature gradients (less than $-5\ \mathrm{K\ m^{-1}}$). A mixture theory (Brown et al., 1997, 1999) has been used to model equilibrium growth metamorphism. The results of the theory were compared to experimental data (Brown et al., 2001). This formulation demonstrated very good correlation with the scarce experimental data for both grain growth and bond growth. A stereology program (Edens and Brown, 1995) was used to measure the microstructure of snow, in this case mean grain size, mean bond size and mean neck length. For a discussion of grain size definition and determination, see also Baunach et al. (2001). The analysis yielded for the grain growth rate, given the sphericity, sp, of the grains:

$$\dot{r}_g(T,t) = \mathrm{sp}\left(A_1 + \frac{A_2}{r_g}\right) e^{A_3(1/T_R - 1/T)}. \quad (1)$$

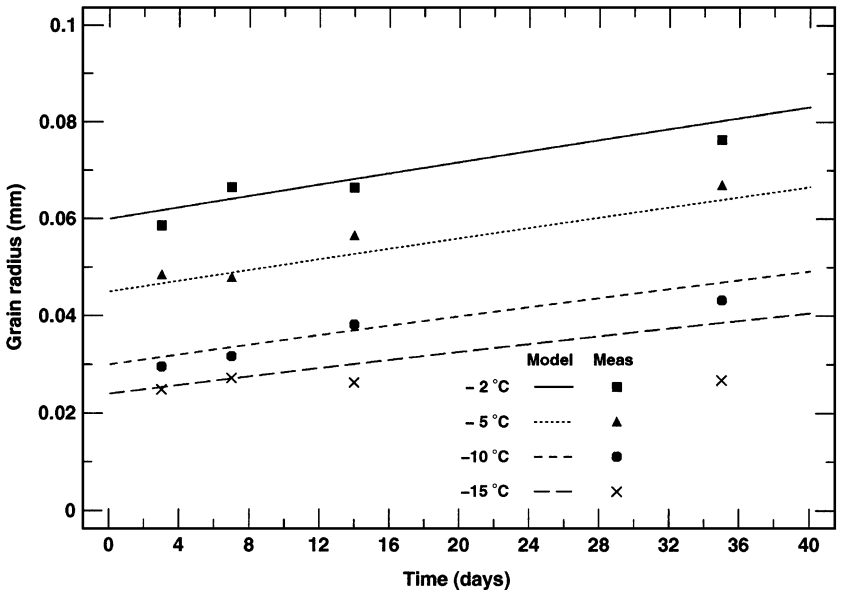

Fig. 3. Comparison of equitemperature grain growth prediction with laboratory data for various temperatures.

T_R is a reference temperature (273.15 K). The data then gives the following values to the coefficients A_1, A_2 and A_3 in Eq. (1) for the rate of change of grain size for snow with a high degree of sphericity:

$$A_1 = 5.9 \times 10^{-12} \quad (\mathrm{m\ s^{-1}})$$

$$A_2 = 9.4 \times 10^{-17} \quad (\mathrm{m^2\ s^{-1}})$$

$$A_3 = 2.9 \times 10^{3} \quad (\mathrm{K}). \tag{2}$$

Mixture theory also suggests an ET bond growth equation of the following form:

$$\dot{r}_b(T,t) = B_1\left(e^{\frac{-B_2}{r_n}} - e^{\frac{-B_2}{r_g}}\right)e^{B_3(1/T_R - 1/T)}, \tag{3}$$

where r_n is the thermodynamic neck radius, which determines the vapor pressure over the ice surface. It is given by:

$$\frac{2}{r_n} = \frac{1}{r_b} - \frac{1}{r_c}, \tag{4}$$

where r_c is the concave radius as shown in Fig. 2:

$$r_c = \frac{r_b^2}{2(r_g - r_b)}. \tag{5}$$

A fit to measured bond growth data results in:

$$B_1 = 1.4 \times 10^{-7} \quad (\mathrm{m\ s^{-1}})$$

$$B_2 = 1.9 \times 10^{-9} \quad (\mathrm{m})$$

$$B_3 = 4.7 \times 10^{3} \quad (\mathrm{K}). \tag{6}$$

A comparison between predicted ET growth and laboratory measurements for different temperatures is given in Figs. 3 and 4 for grains and bonds, respectively. The experiments are described in Brown et al. (2001). The model captures important features of the grain growth and bond growth data and predicts reasonable growth rates.

Eq. (1) states that when the snow becomes fully faceted and then comes under low-temperature gradient conditions, (say $\partial T/\partial z < 1\ \mathrm{K\ m^{-1}}$), grain growth will cease, since faceted surfaces are quite stable and will not undergo changes very quickly. When the grain has a high degree of sphericity, the mean grain

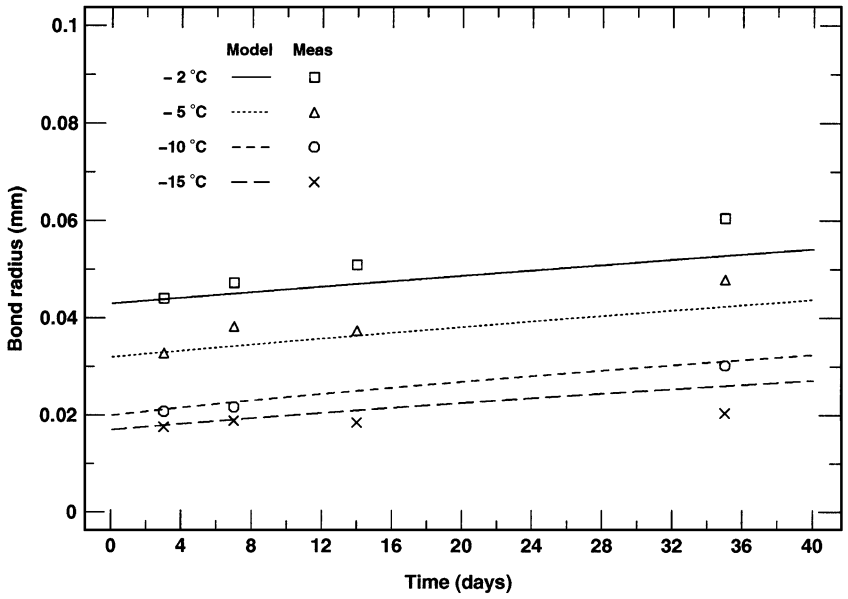

Fig. 4. Comparison of equitemperature bond growth prediction with laboratory data for various temperatures.

size will continue to increase according to the above formulation, since small rounded grains will always be available to provide mass to the larger rounded grains and what faceted surfaces that exist on the grains. If the grain size distribution was completely uniform, grain growth would theoretically cease. However, snow normally has a distribution of different grain sizes that would ensure continued growth over the period of a winter season. The bonds, on the other hand, will continue to grow regardless of the faceting. A small dependence of the growth rate on the state of faceting is expected, however. This dependence is currently not accounted for.

2.1.2. Kinetic growth metamorphism

At even higher growth rates, water vapour gradients between the ice matrix and the pores play a leading role, and recrystallization occurs. Because supersaturation is low, kinetic growth metamorphism is diffusion limited. Kinetic growth metamorphism has long been described as a "hand-to-hand" process where water vapor sublimates off warmer grains to be deposited on colder grains (Giddings and LaChapelle, 1962). This primary source of water vapor seems to be confirmed by long-term observation of kinetic growth metamorphism in Alaskan snow cover (Sturm and Benson, 1997). Many attempts have been made to understand and describe kinetic growth metamorphism from a theoretical point of view (Colbeck, 1983; Gubler, 1985; Arons and Colbeck, 1995), but these models may hardly be incorporated into operational snow cover models. Up to now, the empirical formulation by Marbouty (1980) has shown to be quite successful (Brun et al., 1992), as it includes temperature, temperature gradient as well as density dependence on kinetic grain growth. However, it fails at very large growth rates (Fukuzawa and Akitaya, 1993).

Here, we present a new approach based on simple theoretical considerations as well as on cold laboratory experiments (Baunach et al., 2001; Fierz and Baunach, 2000). The experiments were performed at a mean snow temperature of -10 °C with temperature gradients in the range of -30 to -350 K m^{-1} and densities ranging from 120 to 290 kg m^{-3}.

The driving force of the recrystallization process involved in kinetic growth metamorphism is considered to be water vapor gradient between ice matrix and pore space. The associated water vapor flux j is assumed to obey Fick's law:

$$J_v = -D\frac{\partial \rho_v}{\partial z}, \tag{7}$$

where ρ_v is the water vapor density, z the coordinate along the macroscopic temperature gradient and D, a diffusion coefficient. In the following, vapor flux approximations will be given for the macroscopic vapor flux, i.e. the vertical flux between snow layers or finite elements as well as for the microscopic vapor flux, i.e. the exchange of vapor between grains (or bonds) within one snow layer (element). At present, these formulations are not yet integrated with the global vapor transport equation (Eq. (15), Part I) but are local estimations. Future work will be devoted to have the grain and bond growth formulations dependent on the global vapor transport treatment.

For saturated conditions, the flux J_v may be expressed in terms of temperature T and temperature gradient $\partial T/\partial z$, assuming water vapor to be an ideal gas and using the Clausius–Clapeyron equation:

$$J_v\left(T,\frac{\partial T}{\partial z}\right) = -D_{vs}\frac{p_S(T)}{RT^2}\left[\frac{L}{RT}-1\right]\frac{\partial T}{\partial z} \tag{8}$$

D_{vs} is the diffusion coefficient of water vapor in snow, R_v is the gas constant for water vapor, L, latent heat of sublimation of ice and p_S, water vapor saturation pressure.

Moreover, we consider two sources to contribute to the water vapor supply involved in kinetic growth metamorphism: First, layer-to-layer transport, ΔJ_{L2L}, calculated from the flux (Eq. (8)) difference at the top and the bottom of a layer (element) with thickness Δz, i.e. using the temperature gradients at the boundaries (nodes) of the layer. Second, intra-layer or grain-to-grain flux, J_L, calculated using the temperature gradient at the center of the layer (element). To account for the latter, we consider the ice matrix to be initially a body-centered cubic lattice of lattice constant a. The assumed geometry for the model is given in Fig. 5. All grains within a unit cell are initially cubes with sides $r_g(0)$. The central grain then acts as a source and the vertex grains as sinks (Fig. 5). Because intra-layer flux conserves mass, we may express the lattice constant $a(t)$ as:

$$a(t) = \left(\frac{2f_{gg}r_g(0)^3 + V_{L2L}(t)}{\theta_i(t)}\right)^{1/3}, \tag{9}$$

where θ_i is the volumetric content of ice, V_{L2L} is the time integrated ice volume increase due to layer-to-layer flux and f_{gg} a geometrical factor taking account

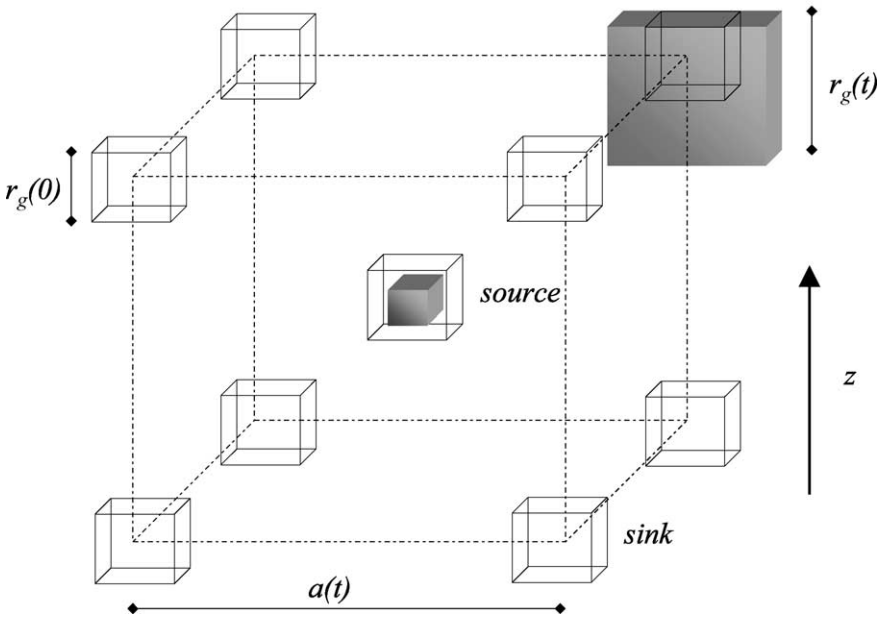

Fig. 5. Assumed lattice geometry for kinetic grain growth model.

of the real grain shape. Based on our observations, grains are allowed to grow as plates, one side remaining fixed at $r_g(0)$, while the other two sides grow as $r_g(t)$. The integrated ice volume increase is approximated for each layer of thickness Δz:

$$V_{L2L}(t) = V_{L2L}(t-\Delta t) + \frac{(a(t-\Delta t))^3}{\rho_i}\frac{\Delta J_{L2L}\Delta t}{\Delta z}, \tag{10}$$

where Δt is the model time increment and ρ_i is the density of pure ice. The growth rate $\dot{r}_g(t)$ is finally expressed as:

$$\dot{r}_g(t) = \frac{a^2(t)J_L(t) + \frac{a^3(t)}{\Delta z}\Delta J_{L2L}(t)}{2f_{gg}\rho_i r_g(0) r_g(t)}. \tag{11}$$

Fig. 6 compares calculated growth rates to the ones observed in our experiments. Average, minimum and maximum grain diameter were obtained by processing images of disaggregated snow samples taken during the experiments (Fierz and Baunach, 2000). Taking a value of $f_{gg}=2$, a good agreement is reached.

The same mechanism is working to grow the bonds between the grains. However, for the bonds between the (larger) grains, it is not the temperature gradient across the whole cell but rather the local (microscale) gradient along the bond (or neck) that determines the vapor flux. Therefore, we first need to determine this local temperature gradient. We again assume a certain geometrical lattice: We replace the cubes in Fig. 5 by two (round) grains each, which are connected by a (vertical) bond. We assume that the bonds grow due to vapor transport from the neighboring grains. Then, analyzing the heat transfer rates through the lattice and using the same concept as Adams and Sato (1993), which is explained in more detail in Section 2.3, we can write the local temperature gradient across a bond as:

$$\frac{\partial T}{\partial z}_{\text{bond}} = \frac{A k_e}{A_g k_i}\frac{\partial T}{\partial z}. \tag{12}$$

Here, A is an average cross-sectional area:

$$A = \frac{1}{3}(A_g + A_b + A_p) = \frac{1}{3}(\pi r_g^2 + \pi r_b^2 + A_p). \tag{13}$$

Eqs. (12) and (13) make use of the cross-sectional areas of the grains, the bonds and the pores. These microstructural parameters are treated below in Section 2.3. The thermal conductivities of snow, k_e, and pure ice, k_i, are also explained in Section 2.3. Using again Eq. (8), the following rate of bond growth is finally obtained:

$$\dot{r}_b(t) = f_{gb}\frac{D_{va}}{\rho_i}\frac{p_v(T)}{RT^2}\left[\frac{L}{RT} - 1\right]\frac{\partial T}{\partial z}_{\text{bond}}. \tag{14}$$

Note that here the diffusion coefficient of water vapor in air is used together with the local gradient. The density-dependent geometrical factor for bond growth, f_{gb}, can be theoretically predicted for a cubic packing of grain–bond–grain units as assumed above:

$$f_{gb} = \frac{r_g^2}{r_b l_n} - \frac{r_b}{2l_n}. \tag{15}$$

Here l_n is the neck length (Eq. (43)). The results discussed in Part III are obtained for a constant value of $f_{gb}=0.35$. An interesting property of this conceptual model of bond growth is that it explains the observational fact that under conditions of high temperature gradients, faceted crystals grow which have a high compression viscosity but a low shear strength. Our model of bond growth is valid for vertically oriented bonds but does not grow horizontal bonds. The mechanical properties in our 1D model are mainly determined by the bond radius.

Fig. 7 compares model predictions of kinetic bond growth with laboratory experimental data. It can be seen that the model predictions are well within the uncertainty of the measurements and that measured and simulated bond growth show similar characteristics.

2.1.3. Grain shape development

The remaining two microstructural parameters, dendricity (dd) and sphericity (sp), are discussed in this section. Our empirical rate equations are based on the French model formulation (Brun et al., 1989, 1992) and adjusted to fit our observational data. New snow is assumed to have a dendricity of 1 and a sphericity of 0.5. In new snow, the main process is the "loss" of dendricity. The rate of change depends

again on the temperature gradient and we distinguish two regimes for the case of dry new snow:

$$\dot{dd}(t) = \begin{cases} -2 \times 10^8 e^{\frac{-6000}{T}}, & \left|\frac{\partial T}{\partial z}\right| \le 5 \frac{K}{m} \\ -2 \times 10^8 e^{\frac{-6000}{T}} \left|\frac{\partial T}{\partial z}\right|^{0.4}, & \left|\frac{\partial T}{\partial z}\right| > 5 \frac{K}{m} \end{cases}, \tag{16}$$

Here $\dot{dd}(t)$ has the unit (1/s). The change of sphericity is made dependent on the change of dendricity: The grains round as they loose their dendricity:

$$\dot{sp}(t) = \begin{cases} -0.3\dot{dd}(t), & \left|\frac{\partial T}{\partial z}\right| \le 5 \frac{K}{m} \\ 0.3\dot{dd}(t), & \left|\frac{\partial T}{\partial z}\right| > 5 \frac{K}{m} \end{cases}. \tag{17}$$

In old and dry snow, the change of sphericity is assumed to be:

$$\dot{sp}(t) = \begin{cases} 5 \times 10^8 e^{\frac{-6000}{T}} \left(5 - \left|\frac{\partial T}{\partial z}\right|\right), & \left|\frac{\partial T}{\partial z}\right| \le 5 \frac{K}{m} \\ -1 \times 10^8 e^{\frac{-6000}{T}} \left|\frac{\partial T}{\partial z}\right|^{0.4}, & \left|\frac{\partial T}{\partial z}\right| > 5 \frac{K}{m} \end{cases}. \tag{18}$$

The sharp transition between the two regimes in Eq. (18) is not supported by theoretical considerations or observational data and Eq. (18) will have to be improved.

2.1.4. Wet snow metamorphism

Wet snow is treated separately since the regime for the change of microstructural parameters changes. Grain growth and changes in sphericity and dendricity are much faster than in dry snow. At present, we only have a rudimentary treatment of wet snow metamorphism which is also based on the works of Brun (1989) and Brun et al. (1989). Brun et al. (1992) presented an empirical relationship for the volume growth of grains as a function of the mass fraction of liquid water, θ_w^m. Expressed as grain radius growth, we use:

$$\dot{r}_g(t) = \frac{4\pi(C_1 + C_2 \theta_w^m(t)^3)}{r_g(t)^2}, \tag{19}$$

where the two empirical constants are: $C_1 = 1.1\ 10^{-3}$ mm day^{-1} and $C_2 = 3.7\ 10^{-5}$ mm day^{-1}. No data or theoretical considerations are currently available for wet snow bond growth. Therefore, we choose a conservative approach and assume that the wet snow bond growth is dominated by pressure sintering. The fast grain growth together with the low viscosity of ice at the melting temperature will cause a significant bond growth due to pressure sintering (Section 2.2) and we model wet snow bond growth by Eq. (28).

The change in dendricity and sphericity for new wet snow are assumed to be:

$$\dot{dd}(t) = -\frac{\theta_w^m(t)^3}{16} \text{ and } \dot{sp}(t) = -0.5\dot{dd}(t). \tag{20}$$

For old wet snow we have:

$$\dot{sp}(t) = \frac{\theta_w^m(t)^3}{16}. \tag{21}$$

Thus, the changes in wet snow are much faster than in dry snow.

2.1.5. Snow type marker and grain classification

Using the four primary parameters of microstructure as discussed above, many important features of the snow in a seasonal snow cover can be described. However, the set of parameters is incomplete in the sense that some of the snow changes that are observed and understood cannot be represented by those parameters. For example, melt–freeze crusts must also be represented. To overcome these shortcomings, we introduce a snow type marker that tracks the history of grain development. For new snow (dendricity>0), the marker is set to 0. The sphericity of new snow is assumed to be 0.5. Therefore, the sphericity might increase or decrease, depending on the temperature conditions in the snow pack: if the sphericity first reaches 1 (and has not previously been 0), 2 is added to the marker (grains become fully rounded); if, however, the sphericity reaches 0 first, 1 is added to the marker (grains become fully faceted). The first wetting of an element (grain) adds 10 to the marker and the first re-freezing adds another 10 (first melt–freeze cycle completed). The marker plays a role in the grain classification (s. below) and is also used to

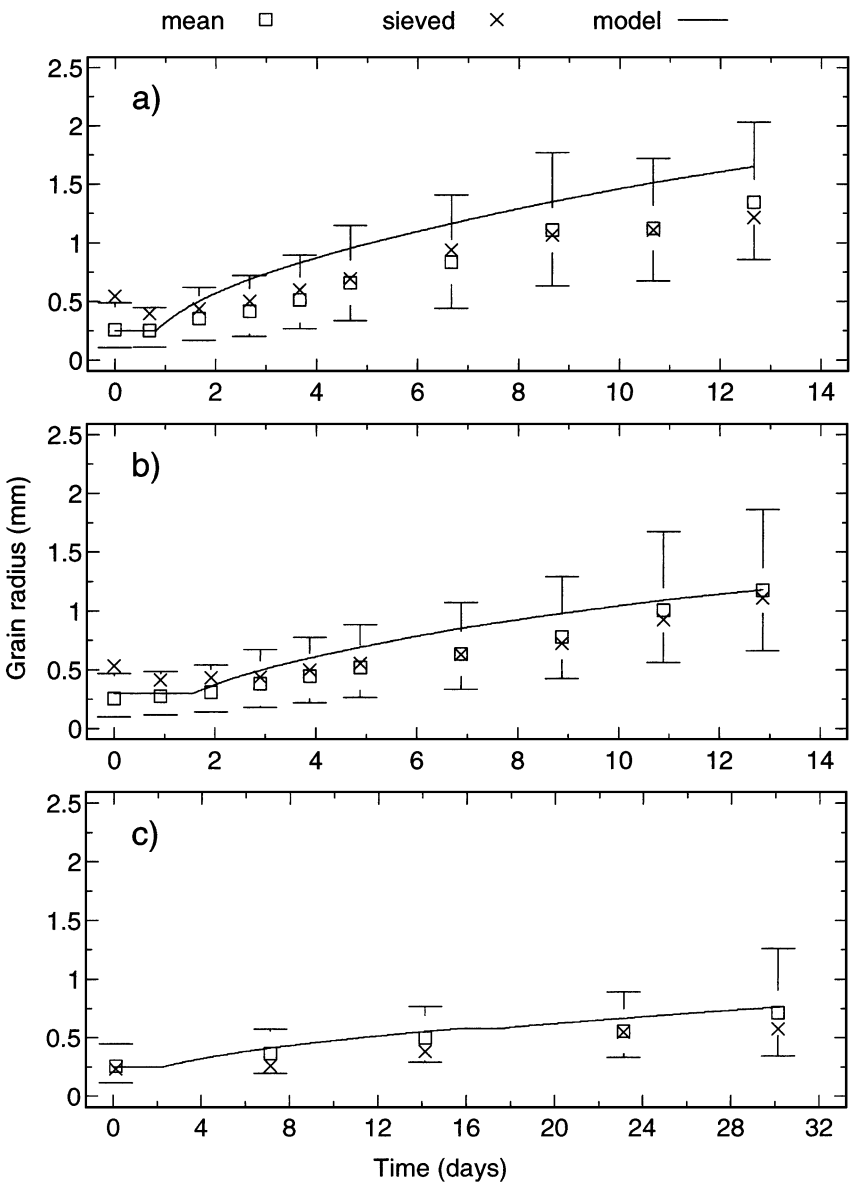

Fig. 6. Comparison of kinetic grain growth prediction with laboratory data for three experiments. 'Mean' values are obtained from processing disaggregated grain images and 'sieved' values from sieving snow samples. Also shown is the range of the measured grain sizes (image processing only). (a) Temperature gradient: -240 K m^{-1}; density: 120 kg m^{-3}. (b) -160 K m^{-1}; 140 kg m^{-3}. (c) -35 K m^{-1}; 210 kg m^{-3}.

limit sphericity changes in the snow pack, i.e. for melt freeze crusts as well as large faceted grains, which are known to be more stable to subsequent rounding.

Fig. 8 is a summary of the grain classification that is performed by SNOWPACK. Note that surface hoar and ice lenses are not part of the classification scheme. The formation of surface hoar is modeled. However, the hoar layer is not treated as a numerical layer but as a layer boundary. Currently, it does not undergo metamorphic development. For the purpose of avalanche warning, the presence of a surface hoar layer needs to be predicted. SNOWPACK predicts the mass

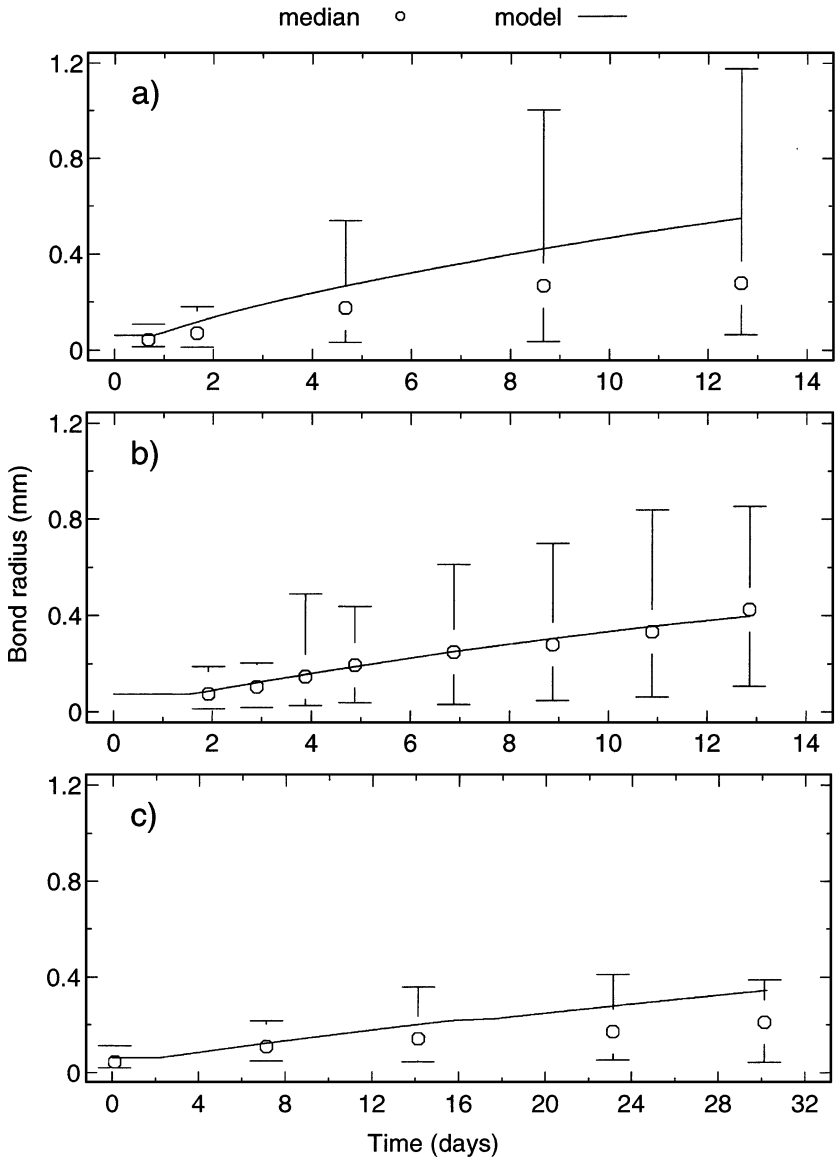

Fig. 7. Comparison of kinetic bond growth prediction with laboratory data for three experiments. 'Median' values are obtained from processing disaggregated grain images. Also shown is the range of the measured bond sizes. (a) Temperature gradient: -240 K m^{-1}; density: 120 kg m^{-3}. (b) -160 K m^{-1}; 140 kg m^{-3}. (c) -35 K m^{-1}; 210 kg m^{-3}.

of surface hoar formed (Part III) and tracks buried surface hoar layers. While it is known that buried surface hoar changes and becomes less dangerous once deeply buried in the snow cover, there exist no quantitative data at present. Therefore, buried surface hoar layers in SNOWPACK persist and only change (disappear) during melt processes. The symbol for ice lenses is used, when the volumetric ice content exceeds 0.7.

2.2. Pressure sintering and viscosity

One of the added features of the snow pack model is the ability to calculate snow pack settlement as it is

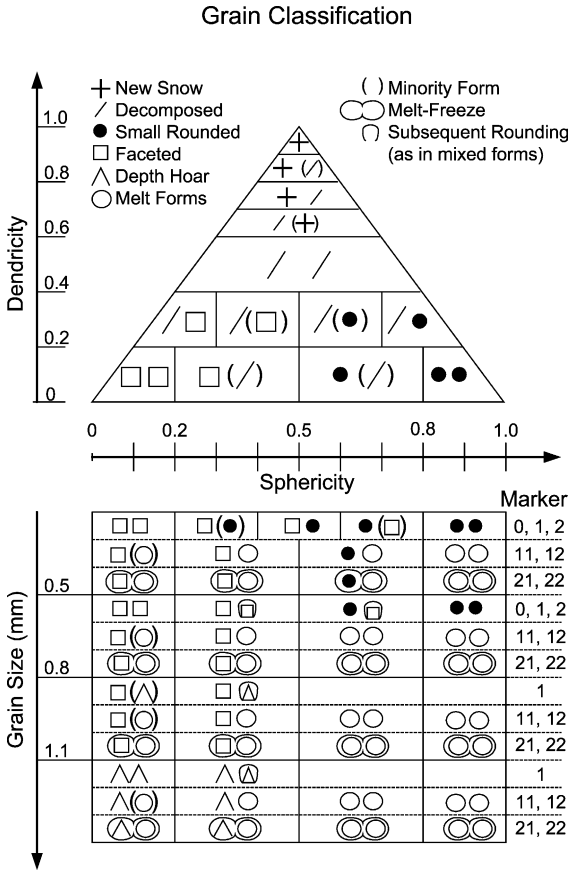

Fig. 8. Grain classification scheme to translate the microstructure parameters into conventional grain types.

affected by the various metamorphism processes. Snow is a viscoelastic material that undergoes large irreversible deformations. In Part I, the settling formulation in SNOWPACK is treated, which needs snow viscosity as a parameter. The material viscosity, η, relates the stress σ to the strain rate $\mathrm{d}\varepsilon/\mathrm{d}t$, when elastic deformations are small as in the case of snow settling (Eqs. (25)–(28), Part I):

$$\dot{\varepsilon} = -\sigma_s/\eta_s, \tag{22}$$

where σ_s is the applied snow pressure (in this case the self-weight of the snow pack). Therefore, low values of viscosity will result with large rates of settlement, while large viscosities will yield low settlement rates. Fig. 1 shows a surface section of well-bonded granular snow with the necks connecting the ice grains depicted by the gray regions. Since the necks are the regions of maximum stress, most of the deformation takes place there. The stresses in the necks may be more than an order of magnitude larger than the stresses in the grains (see also Eq. (26)). The necks may be directly compressed and they can also deform in shear. The result is that under compressive loads, the ice grains move closer to each other, the pores occupy a smaller portion of the snow volume and the density increases. The whole process is called pressure sintering and leads to a bond growth which takes place in addition to the kinetic or ET bond growth.

The calculation of viscosity will be broken into two parts: a nonlinear range and a linear range. This is determined by the properties of ice itself. At low stresses, ice exhibits a nearly linear behavior, and the strain rate ε_i is governed by a relation of the form:

$$\dot{\varepsilon}_i = \sigma/\eta_i. \tag{23}$$

In the nonlinear range, the relationship between stress and strain rate is:

$$\dot{\varepsilon}_i = \sigma^n/\eta_i', \tag{24}$$

where the exponent, n, may vary between 2.0 and 3.5 and the prime in η_i' points to the fact that the viscosity is different from the one in Eq. (23). This is essentially Glen's flow law, and much experimental data place the value of n close to 3.0 (Bartelt and von Moos, 2000). However, it does vary over the full range of stresses due to the fact that different deformation mechanisms become significant at different stress levels. In this development, we will assume n to have a value of 3.0. First, we develop the constitutive relation for the nonlinear range and then finish by developing the linear relationship for the viscosity. The critical stress of 0.4 MPa dividing the linear and nonlinear ranges of material behavior is an ice property. Therefore, whether the behavior of snow is linear or nonlinear is determined by the stress applied to the ice in the necks, not to the snow itself.

The constitutive relationship for snow in this program relates volumetric strain rate to hydrostatic pressure. Since this constitutive law is being used in a one-dimensional snow pack model, this is sufficient. The following development is a simplified version of the formulation developed earlier by Mahajan and Brown (1993). This constitutive formulation includes

the combined effects of pressure sintering (bond growth), intergranular glide, bond fracture with resultant intergranular slip and elastic response. As such, this formulation is a very comprehensive one in that it includes the important deformation mechanisms, represents the material microstructure and can even calculate evolving anisotropy that results from sustained deformation. However, the formulation in its complete form has proven to be too computationally intensive for use in SNOWPACK. Therefore, a simplified version of this constitutive equation is developed here by dropping the portion describing bond fracture and also the portion representing intergranular glide. This latter process, while giving a material response that is somewhat different than that of pressure sintering, can be approximately represented by the sintering mechanism with the appropriate empirical adjustment.

There have been a number of constitutive relations for ice that have been developed. Sinha (1978) proposed that the viscoelastic properties of ice are described by the elastic, delayed elastic and viscous parts. The delayed elastic response is a function of the crystal size of the polycrystalline ice and controls the primary creep properties. We employ only the elastic and viscous parts. The reason for this is that stress states in snow covers normally change slowly or are steady. This is the case even during snowfall since heavy snowfalls add snow at the rate of only 5–10 cm/h. At these rates of deposition, the stresses change slowly enough to remain near a steady-state flow condition. Dynamic loads such as applied by explosives, skiers or cornice falls are not considered here.

2.2.1. Nonlinear range

The steady-state uniaxial strain rate of ice in terms of an applied axial load may be determined by the relation (Sinha, 1978):

$$\dot{\varepsilon}_{\mathrm{i}} = \frac{\sigma^{\mathrm{n}}}{\eta_{\mathrm{i}}'} = \frac{\sigma}{\eta_{\mathrm{i}}^{\mathrm{p}}} = \dot{\varepsilon}_1(T_{\mathrm{R}}, \sigma_1)\mathrm{e}^{\left[\frac{Q}{R}\left(\frac{1}{T_{\mathrm{R}}}-\frac{1}{T}\right)\right]}\left(\frac{\sigma}{\sigma_1}\right)^3. \quad (25)$$

In this equation, $\dot{\varepsilon}_1(T_{\mathrm{R}},\sigma_1)$ is the strain rate at the reference temperature T_{R} and at the unit stress σ_1 and $\eta_{\mathrm{i}}^{\mathrm{p}}$ is a pseudo-linear ice viscosity masking the nonlinear stress dependency. These are determined by experiment, and we set the unit stress to 0.5 MPa and the reference temperature to -10 °C. The corresponding unit strain rate is 1.76×10^{-7}/s. Q is an activation energy of 67 kJ mol^{-1} and R the universal gas constant. The equation is considered to be valid for ice stresses in excess of 0.4 MPa.

Eq. (25) can be used to determine the strain rate in the necks once the stresses in the neck can be related to the stresses applied to the snow. The relationship between the neck stress and the snow stress can be derived by using a variational approach (Mahajan and Brown, 1993) to relate the work done within the necks to the work done by the applied global stress work. This approach yields:

$$\sigma_{\mathrm{n}} = \frac{4}{N_3\theta_{\mathrm{i}}}\left(\frac{r_{\mathrm{g}}}{r_{\mathrm{b}}}\right)^2\sigma_{\mathrm{s}}. \quad (26)$$

In this case, we are assuming a hydrostatic pressure, σ_{s}, is applied to the snow. The neck stress, σ_{n}, is related to the snow stress by the square of the ratio of the grain size to bond size, the 3-D coordination number, N_3 (Eq. (37)), and the snow volume fraction. This can produce a considerable magnification factor for the neck stress over the snow stress. An extreme case for snow would include a density of 120 kg/m^3, an $r_{\mathrm{g}}/r_{\mathrm{b}}$ ratio of 7.0 and a coordination number of 2.0. In this case, the neck stress can be seen to be almost 750 times as large as the snow stress. A snow stress of 550 Pa would induce nonlinear deformation in the necks. This would correspond to snow buried less than 0.5 m below the surface.

Combining Eqs. (25) and (26) gives:

$$\dot{\varepsilon}_{\mathrm{n}} = \dot{\varepsilon}_1(T_{\mathrm{R}}, \sigma_1)\mathrm{e}^{\left[\frac{Q}{R}\left(\frac{1}{T_{\mathrm{R}}}-\frac{1}{T}\right)\right]}\left[\frac{4\sigma_{\mathrm{s}}}{N_3\theta_{\mathrm{i}}\sigma_1}\left(\frac{r_{\mathrm{g}}}{r_{\mathrm{b}}}\right)^2\right]^3. \quad (27)$$

This is the strain rate in a neck. The neck has a length l_{n}, and the grains have a mean radius of r_{g}. The rate of bond growth due to pressure sintering, $\dot{r}_{\mathrm{b}}^{\mathrm{PS}}$, follows immediately from Eq. (27) and is added to the kinetic (Eq. (11)) or ET (Eq. (3)) growth rate:

$$\dot{r}_{\mathrm{b}}^{\mathrm{PS}} = C_{\mathrm{PR}} r_{\mathrm{b}} \dot{\varepsilon}_{\mathrm{n}}. \quad (28)$$

Here C_{PR} is the plastic Poisson's ratio which is set to 0.5.

To relate the strain rate in the necks to the overall (volumetric) strain rate of the snow, we turn to the

definition of the deformation velocity gradient and assume a small but finite strain:

$$\dot{\varepsilon} = \frac{\mathrm{d}u}{\mathrm{d}z} \approx \frac{\Delta u}{\Delta z} \approx \frac{l_\mathrm{n}\dot{\varepsilon}_\mathrm{n}}{\Delta z} \approx \frac{l_\mathrm{n}\dot{\varepsilon}_\mathrm{n}}{2r_\mathrm{g} + l_\mathrm{n}}. \tag{29}$$

Here u is the deformation velocity. The resulting volumetric constitutive relation becomes:

$$\dot{\varepsilon} = \left[\frac{l_\mathrm{n}}{2r_\mathrm{g} + l_\mathrm{n}}\right]\dot{\varepsilon}_1(T_\mathrm{R}, \sigma_1)\mathrm{e}^{\left[\frac{Q}{R}\left(\frac{1}{T_\mathrm{R}} - \frac{1}{T}\right)\right]} \times \left[\frac{4F_\eta\sigma_\mathrm{s}}{N_3\theta_\mathrm{i}\sigma_1}\left(\frac{r_\mathrm{g}}{r_\mathrm{b}}\right)^2\right]^3. \tag{30}$$

In the above, the term F_η is an empirical constant used to fit the equation to the experimental data. This model is a simplistic one that does not include the effect of intergranular glide or the formation of new bonds in the densification process, as indicated earlier. However, since the constitutive relation governing the shearing deformations in the necks is similar to the one given above, rather than adding an additional deformation process to the constitutive relation, the constant F_η can be used to augment the densification rate over what the above equation would predict. Other factors that would also require an empirical adjustment factor include the fact that the material making up the necks have a high degree of lattice imperfections and interstitial voids, since necks invariably contain a grain boundary and hence have a high degree of crystal misalignment. A high density of lattice imperfections serves to decrease the material resistance to flow. For both of these effects, intergranular gliding and lattice imperfections, an inverse dependency on snow density is to be expected. From our experimental data, which are discussed in more detail in Part III, we also found that the dependency of F_η on the density of snow is nonlinear. In addition, we have to include the effect of liquid water, which will decrease the viscosity. From our data evaluation studies, we suggest to use the following relationship for F_η:

$$F_\eta = \frac{0.4}{\theta_\mathrm{i}} + 3.2\frac{\mathrm{e}^x}{1+\mathrm{e}^x} + 35\theta_\mathrm{w}, \qquad \text{where} \quad x = \frac{0.3 - \theta_\mathrm{i}}{0.05}. \tag{31}$$

The second term describes a transition at densities around 300 kg m^{-3}. For higher densities, a different regime results with an overproportionally lower correction, $F_{\eta'}$ which is used to increase the viscosity.

The viscosity then becomes:

$$\eta_\mathrm{s} = \left\{\left[\frac{l_\mathrm{n}}{2r_\mathrm{g} + l_\mathrm{n}}\right]\dot{\varepsilon}_1(T_\mathrm{R}, \sigma_1)\mathrm{e}^{\left[\frac{Q}{R}\left(\frac{1}{T_\mathrm{R}} - \frac{1}{T}\right)\right]} \times \left[\frac{4F_\eta}{N_3\theta_\mathrm{i}\sigma_1}\left(\frac{r_\mathrm{g}}{r_\mathrm{b}}\right)^2\right]^3\sigma_\mathrm{s}^2\right\}^{-1} \tag{32}$$

For stresses that produce neck stresses in excess of 0.4 MPa, the viscosity is dependent upon the second power of the applied snow pressure σ_s.

2.2.2. Linear range

When the stresses drop below the value that makes the neck stress less than 0.4 MPa, we assume the ice behaves as a linear viscoelastic material. The steady-state strain rate of the ice in the necks is then given by the relation:

$$\dot{\varepsilon}_\mathrm{n} = \frac{\sigma_\mathrm{n}}{\eta_0} \tag{33}$$

where the linear ice viscosity is given by η_0 and is not stress dependent. It of course may be a function of temperature and the material microstructure. Utilizing Eqs. (26) and (29), the snow viscosity in the linear range becomes:

$$\eta_\mathrm{s} = \frac{N_3\theta_\mathrm{i}}{4}\left(\frac{r_\mathrm{b}}{r_\mathrm{g}}\right)^2\left(\frac{l_\mathrm{n} + 2r_\mathrm{g}}{l_\mathrm{n}}\right)\eta_0. \tag{34}$$

The value of η_0 can now be determined by requiring that at the critical neck stress of 0.4 MPa, the viscosity given by Eqs. (32) and (34) must provide a smooth transition from the linear range to the nonlinear range, i.e. that there is no jump in deformation rate across the critical neck stress. Therefore, at the critical neck stress of $\sigma_\mathrm{n} = \sigma_\mathrm{ncrit} = 0.4$ MPa, we equate the linear viscosity η_0 in Eq. (34) and the pseudo-linear ice viscosity, $\eta_\mathrm{i}^\mathrm{p}$, in Eq. (25). This gives for η_0:

$$\eta_0 = \frac{\sigma_1^3}{\dot{\varepsilon}_1(T_\mathrm{R}, \sigma_1)F_\eta^3\sigma_\mathrm{ncrit}^2}\mathrm{e}^{-\frac{Q}{R}\left[\frac{1}{T_\mathrm{R}} - \frac{1}{T}\right]}. \tag{35}$$

The corresponding rate of bond growth due to pressure sintering is obtained according to Eq. (28) from Eq. (33) with Eq. (26) and Eq. (35).

The microstructure-based viscosity as described above is applied to old dry and wet snow, i.e. snow which has already lost its dendricity. For new snow, an empirical relationship of the Kojima (1975) type is employed:

$$\eta_s = 0.007\rho^{(4.75-T_C/40)}. \quad (36)$$

The coefficients have been chosen such that measured settling rates of fresh snow at a variety of sites in the Swiss Alps can be reproduced. An example of an evaluation of the viscosity formulation examining settling rates during the course of a whole winter in a natural snow cover is Fig. 9. It can be seen that in general the settling curves are well predicted. Small deviations in settling rates of individual layers sum up to a larger total deviation in the upper part of the snow cover. More details are given in Fierz and Lehning (2001). In addition, several mass balance evaluations, which critically depend on a correct viscosity formulation, are found in Part I.

2.3. Thermal conductivity

To solve the bulk temperature equation (Eq. (3), Part I), an estimation of the thermal conductivity of snow is required. The thermal conductivity must be parameterized including all heat transfer processes not explicitly modeled. Such processes are vapor transport across a pore space, or ventilation. The following model is developed extending the work of Adams and Sato (1993), Sato et al. (1994) and Edens and Brown (1995). Snow is modeled as a system of ice grains and pores in series and parallel with each other. Some of the heat conduction is through the ice, where the effect of the constriction induced by bonds and necks is taken into account: q_i, solid ice conduction from one grain through a bond/neck into a neighboring ice grain. Another portion of the heat conduction is due to the transfer of heat from one ice grain across a pore space and then onto another ice grain: q_{ip}, series conduction of heat through a grain, then across a pore and again into another grain. The third portion of the transfer is associated with heat transfer within a pore which is large enough that the upper or lower bounding ice grain can be ignored: q_p, conduction purely across a pore. Radiation heat transfer across the pore

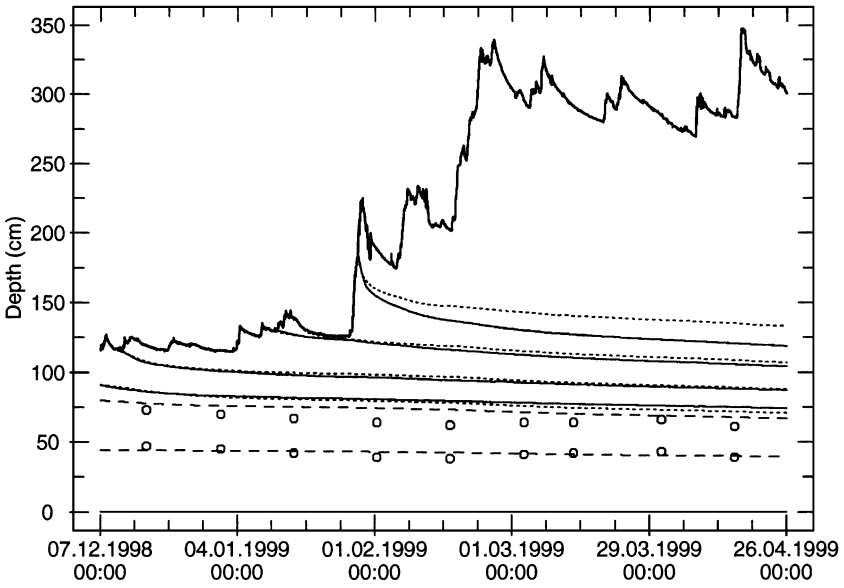

Fig. 9. Comparison between measured and modelled settling rates of individual snow layers during the course of the avalanche winter 1998–1999 at the Versuchsfeld Weissfluhjoch. Solid lines and open circles are measured and dashed lines are simulated.

space is not included as a significant factor. Brandt and Warren (1997) have shown that such transfer is not significant. This model is extended to include the effect of liquid water in the pores. It is assumed that liquid water fills small pores as well as concave neck constrictions and therefore a forth portion of heat conduction is introduced: q_{iw}, series conduction of heat through a grain, then across a pore (partly) filled with water and again into another grain. The capacity of the snow to hold liquid water is small enough that the larger pores will drain and are free of water.

It is assumed that the relative roles of these four types of conduction are affected by the material microstructure. Fig. 10 gives a schematic of the types of conduction, and the physical model used for this is given in Fig. 11. This is a simplistic schematic of how the three modes of conduction are modeled. These modes of conduction will be determined in terms of the material microstructure. For instance, measurements by Edens and Brown (1991) have determined the variation of the three-dimensional coordination number with density and fitted the equation:

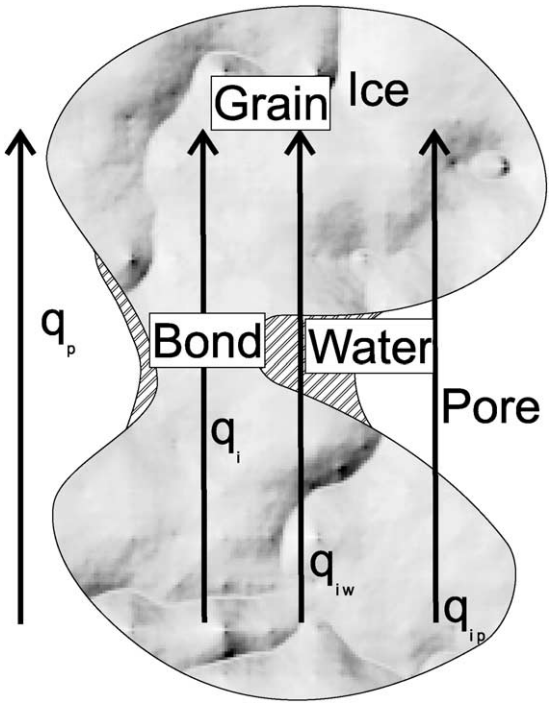

Fig. 10. Types of heat conduction modes in the SNOWPACK conductivity model.

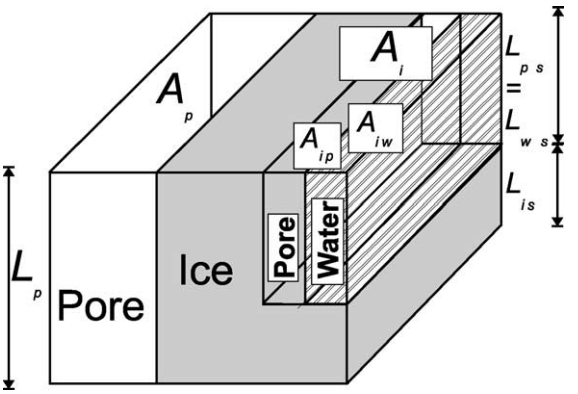

Fig. 11. Schematic for developing heat conduction model. The schematic presents the area (A) and length (L) parameters used in the conduction model.

$$N_3 = 1.43 - 7.56 \times 10^{-5}\rho_s + 5.15 \times 10^{-5}\rho_s^2 - 1.73 \times 10^{-7}\rho_s^3 + 1.81 \times 10^{-10}\rho_s^4. \quad (37)$$

It does not provide any effect that metamorphism has on N_3, but it is not at all clear that metamorphism has any strong effect on coordination number. The primary effect of metamorphism probably lies with the degree of isotropy of bonding and the bond/grain size ratio.

We start with the work of Adams and Sato (1993) and write for the effective conductivity:

$$k_e = \frac{n_{ca}}{n_{cl}}\left[\frac{\pi^2 r_b k_i N_3}{32} + \frac{k_a k_{ap} A_{ip}}{L_{is}k_{ap} + L_{ps}k_i} + \frac{k_a A_p}{L_p}\right]. \quad (38)$$

The conductivity, k_{ap} is the conductivity in the pore space resulting from the combined effects of direct conduction of heat (k_a) and the transport of latent heat. k_{ap} has the value:

$$k_{ap} = k_a + \frac{LD_{va}P}{RT(P-p_v)}\cdot\frac{\partial p_v}{\partial T} \approx k_a + \frac{L^2 D_{va} P p_v}{R^2 T^3 (P-p_v)}. \quad (39)$$

We introduce as a first change to the Adams–Sato formulation a different conductivity of the pore space in parallel to the series and solid heat conduction. In

their formulation, they have ignored the transport of latent heat in the pore and have included it only in the series conduction of heat. The pores, regardless of whether it is the pore situated vertically between two adjacent grains or the pore in parallel to the grains, will have a temperature-dependent vapor at or near saturation. As a consequence, under the influence of a temperature gradient, a vapor pressure gradient will be established with the result that this gradient will push vapor in the direction of the gradient with the result that latent heat will be transferred. The conductivity model is therefore modified to the following:

$$k_e = \frac{n_{ca}}{n_{cl}}\left[\frac{\pi^2 r_b k_i N_3}{32} + \frac{k_a k_{ap} A_{ip}}{L_{is}k_{ap} + L_{ps}k_i} + \frac{k_{ap}A_p}{L_p}\right]. \quad (40)$$

In this equation, the conductivity k_a in the pore conduction term has been replaced by the conductivity k_{ap}. This conductivity term has included in it the effect of latent heat transfer. Therefore, in this model, any conduction of heat which occurs in the pore includes the transport of vapor. It should be pointed out that convective heat transfer is not included, but this is appropriate, since convective heat transfer is normally not included in calculations of material conductivity. In Part III, we present a wind pumping parameterization and how this affects heat transfer.

As a second and more important alteration, the effect of liquid water is introduced in the above model. First, we assume that any liquid water fills the smaller pores or neck constrictions between the grains (Fig. 10). The series conduction, q_{ip}, is thus reduced and replaced by the series conduction, q_{iw}. Using the same arguments as Adams and Sato (1993), the effective conductivity becomes:

$$k_e = \frac{n_{ca}}{n_{cl}}\left[\frac{\pi^2 r_b k_i N_3 F_k}{32} + \frac{k_a k_{ap} A_{ip}}{L_{is}k_{ap} + L_{ps}k_i} + \frac{k_a k_w A_{iw}}{L_{is}k_w + L_{ws}k_i} + \frac{k_{ap}A_p}{L_p}\right]. \quad (41)$$

For the same reasons as in the viscosity formulation (Section 2.1.1), we have to include here in the first term, which describes the heat conduction grain–bond–grain, the empirical correction factor F_k. Similar to the correction introduced in the viscosity formulation, we also find here a regime transition around a snow density of 300 kg m^{-3} and we can use an analogous description of this transition:

$$F_k = 3.5 + 1.6\frac{e^{-x}}{1 + e^{-x}}. \quad (42)$$

Here x is defined by Eq. (31). The microstructural variables that are used in the conductivity model in Eq. (41) include n_c (number of grains per unit volume), N_3 (3-D coordination number), n_{cl}, (number of grains per unit length intercepted per unit length), n_{ca} (number of grains per unit area), A_{ip} (cross-sectional area for series conduction in pores), A_{iw} (cross-sectional area for series conduction in water), A_p (pore cross-sectional area), L_p (mean pore length), L_{is} (ice series length), L_{ps} (pore series length) and L_{ws} (water series length). A basic quantity is the neck length, l_n. For the geometry in Fig. 2, the neck length is:

$$l_n = \frac{2r_g r_b^2}{2r_g(r_g - r_b) + r_g r_b^2}. \quad (43)$$

The mean pore length is approximated by considering the fraction of solid ice mass volume to the snow mass volume:

$$L_p = \sqrt[3]{\frac{4/3\pi r_g^3}{\theta_i^m}}. \quad (44)$$

Here, θ_i^m, is the mass fraction of ice. As shown in Fig. 11, L_p would normally have a value approximated by the inverse of the number of grains per unit length. The mean pore length is closely related to n_c, n_{cl} and n_{ca} (Fig. 11):

$$n_{cl} = \frac{1}{L_p}, \quad (45)$$

$$n_c = \frac{1}{L_p^3} \text{ and} \quad (46)$$

$$n_{ca} = n_{cl}^2. \quad (47)$$

The number of grains intercepted per unit length is assumed to be the cube root of the number per unit volume. The number of grains per unit area is related in a similar fashion to the number per unit volume. Such relationships for n_{cl} and n_{ca} are probably not

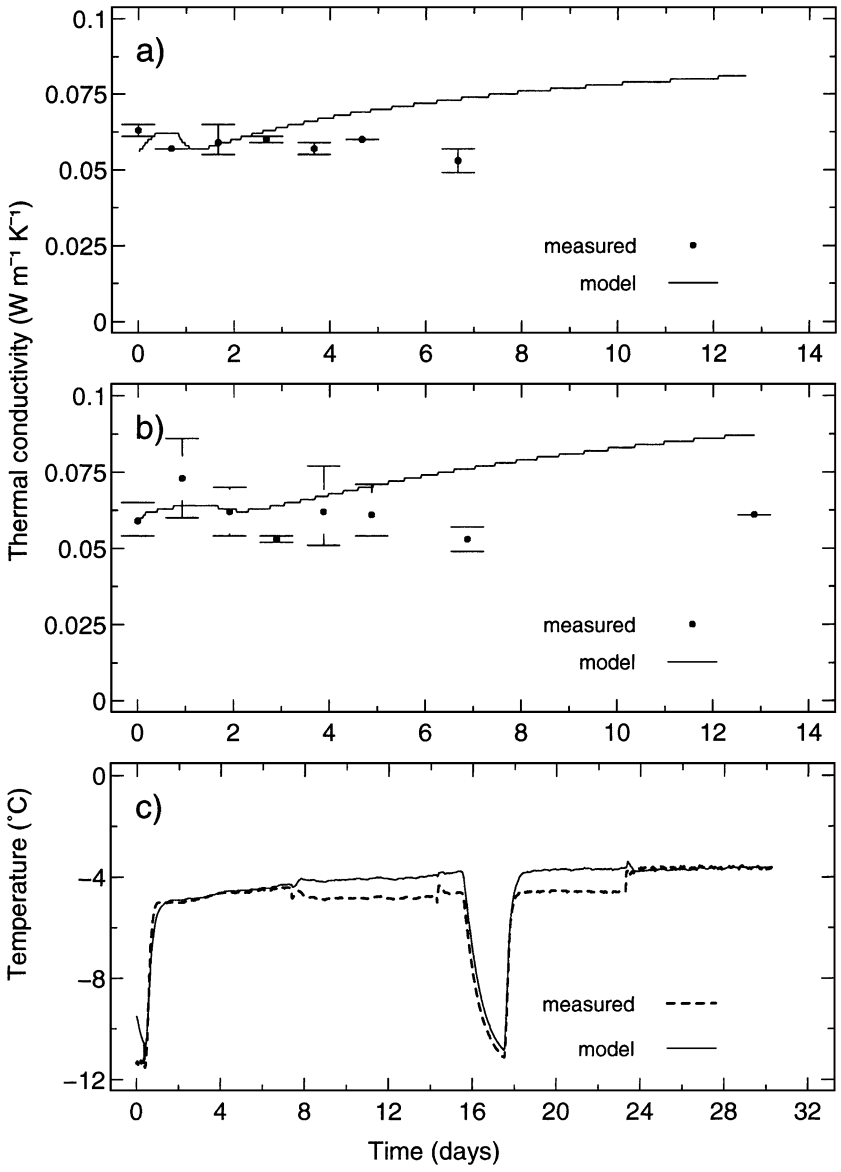

Fig. 12. Comparison of predicted thermal conductivities with laboratory data for two experiments (a and b) as well as measured and modeled temperatures for another experiment (c). Temperature changes due to either establishing or relaxing an imposed temperature gradient are well reproduced. (a) Temperature gradient: -240 K m^{-1}; density: 120 kg m^{-3}. (b) -160 K m^{-1}; 140 kg m^{-3}. (c) -35 K m^{-1}; 210 kg m^{-3}.

strong functions of grain shape, so the variation of these variables with density should be fairly accurate. The values of L_{ps} and L_{is} will be assumed to have the values:

$$L_{ps} = L_{ws} = L_p - r_g$$

$$L_{is} = r_g. \tag{48}$$

The cross-sectional area of the pores is directly related to that of the ice grains. From stereology theory, the pore volume fraction, θ_a, is also equal to the area fraction of the pores, θ_a^a:

$$\theta_a = \theta_a^a = 1 - \theta_i - \theta_w. \tag{49}$$

In addition, the ice volume fraction is also very closely approximated by the ice area fraction:

$$\theta_i = \theta_i^a. \tag{50}$$

In a cell of volume V and cross-sectional area A perpendicular to the direction of heat transfer, we have therefore for the ice and pore cross-sectional areas, A_i and A_p:

$$A_i = \theta_i A$$

$$A_p = \theta_a A = (1 - \theta_i - \theta_w)A. \tag{51}$$

This can be expressed as:

$$A_p = (1 - \theta_i - \theta_w)\frac{A_i}{\theta_i} = (1 - \theta_i - \theta_w)\frac{\pi r_g^2}{\theta_i}. \tag{52}$$

Each cell considered in the Adams–Sato model contains one grain. The cell may (in fact usually does) have a dimension larger than the grain diameter, since the cells must also contain all of the pore space separating the grains. The series cross-sectional area is taken to be the cross-sectional area of a particle minus the bond cross-sectional area. This gives a direct measure of the free surface area available for transfer of heat to the grain surface, across the connecting pore space to the adjoining grain. In case of liquid water in the snow cover, the corresponding cross-sectional area, A_{iw}, is according to the arguments presented above subtracted:

$$A_{ip} = \pi(r_g^2 - r_b^2) - A_{iw}. \tag{53}$$

The cross-sectional area for liquid water is obtained from the schematic model (Fig. 11):

$$A_{iw} = \frac{\theta_w}{L_{ws}} L_p (A_p + \pi r_g^2). \tag{54}$$

It should be noted that in the above model, A_{ip} and A_{iw} are included in the ice cross-sectional area, A_i (Fig. 11). For any realistic values of grain size, bond size and liquid water content, the following relationships will be fulfilled:

$$A_{iw} < A_{ip}, \text{ and } A_{iw} + A_{ip} < A_i. \tag{55}$$

The model prediction of thermal conductivity is compared to laboratory results for two experiments in Fig. 12a and b. For the third experiment, no direct measurements of conductivity are available and Fig. 12c shows the predicted and measured temperature development during the experiment. Note that temperature changes due to either establishing or relaxing an imposed temperature gradient are well simulated.

3. Conclusions

A complete description of the microstructure and metamorphism model used by SNOWPACK is presented including a classification scheme to predict the conventional grain types. Of particular importance is that the important parameter bond size is included in the description of microstructure. This is a prerequisite to model the two bulk properties viscosity and thermal conductivity as a function of those microstructure parameters and to proceed into the field of predicting further mechanical properties such as snow stability.

The microstructure-based models of viscosity and thermal conductivity are a complex and adequate description for natural snow. However, they still need to be calibrated against observational data. The necessary complexity of the empirical corrections required indicates that still some important parts are missing in our description of snow microstructure. The authors mention three possible reasons for this shortcoming: First, we describe snow on the basis of material properties of ice and neglect the fact that the individual grains and bonds contain imperfections and are not made of pure ice too. Second, our model does not include the process of intergranular glide. Third, the effect of liquid water on the viscosity is also not included but parameterized only. In this sense, we conclude that research on snow microstructure has only begun and needs to be continued.

On the other hand, an important step forward has been made by introducing the correct physical interactions into SNOWPACK. Microstructure, temperature and settling interact with each other. For example, an increase in metamorphic bond growth increases also heat conduction and decreases settling. Increased heat conduction decreases the temperature gradient and therefore metamorphic bond growth. At the same time, the decreased settling decreases the rate of pressure sintering such that the bonds grow less due

to this effect. These (and other) feedback mechanisms are correctly represented in SNOWPACK.

Acknowledgements

We thank Walter Ammann and the Board of the Swiss Federal Institutes of Technology for supporting the work. We are very grateful to Matthew Sturm for his pre-review. His big effort and comments improved the papers. Part of the work was accomplished while ML was a visiting scientist at MSU. Ed Adams, Ladean McKittrick, Peter Gauer, Major Miller and Scott Schmidt contributed in various ways.

Appendix A. List of symbols

Symbol	Description	Unit
A	(Average) Cross-sectional area	m^2
A_b	Cross-sectional area of bonds	m^2
A_i	Cross-sectional area of ice (grains)	m^2
A_{ip}	Cross-sectional area for series conduction (pore and ice)	m^2
A_{iw}	Cross-sectional area for series conduction (water and ice)	m^2
A_p	Cross-sectional area of pore space	m^2
A_1	Empirical constant	$m\ s^{-1}$
A_2	Empirical constant	$m^2\ s^{-1}$
A_3	Empirical constant	K
a	Lattice constant	m
B_1	Empirical constant	$m\ s^{-1}$
B_2	Empirical constant	m
B_3	Empirical constant	K
C_1	Empirical constant	$mm\ day^{-1}$
C_2	Empirical constant	$mm\ day^{-1}$
C_{PR}	Poisson ratio	
D	Diffusion coefficient	$m^2\ s^{-1}$
D_{vs}	Diffusion coefficient of water vapor in snow	$m^2\ s^{-1}$
D_{va}	Diffusion coefficient of water vapor in air	$m^2\ s^{-1}$
dd	Snow dendricity	[0–1]
$\dot{dd}$	Snow dendricity rate	s^{-1}
Δj_{L2L}	Net water vapor flux from layer to layer	$kg\ m^{-2}\ s^{-1}$

Appendix A (*continued*)

Symbol	Description	Unit
ε	Strain	
$\dot{\varepsilon}$	Strain rate	s^{-1}
$\dot{\varepsilon}_1$	Reference (unit) strain rate value	s^{-1}
$\dot{\varepsilon}_i$	Strain rate in pure ice	
$\dot{\varepsilon}_n$	Strain rate in the necks	
F_η	Empirical factor for viscosity	
F_k	Empirical factor for grain–bond–grain conductivity	
f_{gg}	Geometrical factor in kinetic grain growth model	
f_{gb}	Geometrical factor in kinetic bond growth model	
η_s	Viscosity of snow	Pa s
η_i, η_i'	Viscosities of pure ice	Pa s
η_i^p	Pseudo-linear viscosity of pure ice	Pa s
j	Water vapor flux	$kg\ m^{-2}\ s^{-1}$
j_L	Water vapor flux within one layer	$kg\ m^{-2}\ s^{-1}$
k_i	Thermal conductivity of pure ice	$W\ m^{-1}\ K^{-1}$
k_a	Thermal conductivity of air	$W\ m^{-1}\ K^{-1}$
k_{ap}	Thermal conductivity of pores including the effect of transport of latent heat	$W\ m^{-1}\ K^{-1}$
k_e	Effective thermal conductivity of snow	$W\ m^{-1}\ K^{-1}$
k_w	Thermal conductivity of liquid water	$W\ m^{-1}\ K^{-1}$
L	Latent heat of sublimation	$J\ kg^{-1}$
L_{is}	Series grain length for ice	m
L_p	Mean pore length	m
L_{ps}	Series pore length (air)	m
L_{ws}	Series pore length (water)	m
l_n	Neck length	m
N_3	Three dimensional coordination number	
n	Exponent of Glen's flow law	
n_c	number of grains per unit volume	m^{-3}
n_{ca}	number of grains per unit area (horizontal)	m^{-2}
n_{cl}	number of grains intercepted per unit length (vertical)	m^{-2}
P	Total atmospheric air pressure	Pa
p_v	Water vapor partial pressure	Pa
p_S	Water vapor saturation pressure	Pa
Q	Empirical value for an activation energy	$kJ\ mol^{-1}$
q_i	Heat flux through ice lattice	$W\ m^{-2}$
q_{ip}	Heat flux grain–pore (air)–grain (series conduction)	$W\ m^{-2}$

(*continued on next page*)

Appendix A (*continued*)

Symbol	Description	Unit
q_{iw}	Heat flux grain–pore (water)–grain (series conduction)	W m^{-2}
q_p	Heat flux through (large) pore	W m^{-2}
R	Universal gas constant	J mol^{-1} K^{-1}
R_v	Specific gas constant for water vapor	m^2 s^{-2} K^{-1}
r_b	Bond radius	m
$\dot{r}_b$	Bond growth rate	m s^{-1}
$\dot{r}_b^{PS}$	Bond growth rate due to pressure sintering	m s^{-1}
r_g	Grain radius (or grain plate diameter)	m
$\dot{r}_g$	Grain growth rate	m s^{-1}
r_c	Concave neck radius	m
r_n	Thermodynamic neck radius	m
ρ_s	Density of snow	kg m^{-3}
ρ_i	Density of pure ice	kg m^{-3}
ρ_v	Water vapor density	kg m^{-3}
sp	Snow sphericity	[0–1]
$\dot{sp}$	Snow sphericity rate	s^{-1}
σ	Stress	Pa
σ_1	Reference (unit) stress value	Pa
σ_i	Stress applied to pure ice	Pa
σ_n	Uniaxial stress in the necks	Pa
σ_{ncrit}	Critical stress in the necks	Pa
σ_s	Overburden stress applied to snow	Pa
T	Temperature	K
T_C	Temperature	°C
T_R	Reference temperature	K
t	Time	s
θ_a	Volume fraction of air	
θ_i	Volume fraction of ice	
θ_w	Volume fraction of liquid water	
θ_a^a	Area fraction of air (pores)	
θ_i^a	Area fraction of ice	
θ_i^m	Mass fraction of ice	
θ_w^m	Mass fraction of liquid water	
u	Deformation velocity	m s^{-1}
V	Volume	m^3
V_{L2L}	Time integrated ice volume increase due to Δj_{L2L}	m^3
x	Dummy variable	
z	Vertical coordinate	m

References

Adams, E.E., Sato, A., 1993. Model for effective thermal conductivity of dry snow cover composed of uniform spheres. Ann. Glaciol. 18, 300–304.

Arons, E.M., Colbeck, S.C., 1995. Geometry of heat and mass transfer in dry snow: a review of theory and experiment. Rev. Geophys. 33 (4), 463–493.

Bartelt, P.B., Lehning, M., this issue. A physical SNOWPACK model for Avalanche Warning: part I. Numerical Model. Cold Reg. Sci. Technol.

Bartelt, P.B., von Moos, M., 2000. Triaxial tests to determine snow viscosity. Ann. Glaciol. 31, 457–462.

Baunach, T., Fierz, C., Satyawali, P.K., Schneebeli, M., 2001. A model for kinetic grain growth. Ann. Glaciol. 32, 1–6.

Brandt, R.E., Warren, S.G., 1997. Temperature measurements and heat transfer in near-surface snow at the South Pole. J. Glaciol. 43, 339–351.

Brown, R.L., Edens, M.Q., Barber, M., Sato, A., 1997. Equitemperature metamorphism of snow. In: Izumi, M., Nakamura, T., Sack, R.L. (Eds.), Snow Engineering: Recent Advances, Proceedings of the Third International Conference on Snow Engineering, Sendai, Japan, 26–31 May 1996. A.A. Balkema, Rotterdam, pp. 41–48.

Brown, R.L., Edens, M.Q., Barber, M., 1999. Mixture theory of mass transfer based upon microstructure. Def. Sci. J. 49 (5), 363–370.

Brown, R.L., Satyawali, P.K., Lehning, M., Bartelt, P., 2001. Modeling the changes in microstructure during metamorphism. Cold Reg. Sci. Technol. 33, 91–101.

Brun, E., 1989. Investigation on wet-snow metamorphism in respect of liquid-water content. Ann. Glaciol. 13, 22–26.

Brun, E., Martin, E., Simon, V., Gendre, C., Coléou, C., 1989. An energy and mass model of snow cover suitable for operational avalanche forecasting. J. Glaciol. 35, 333–342.

Brun, E., David, P., Sudul, M., Brugnot, G., 1992. A numerical model to simulate snow cover stratigraphy for operational avalanche forecasting. J. Glaciol. 38, 13–22.

Colbeck, S.C., 1983. Theory of metamorphism of dry snow. J. Geophys. Res. 88 (C9), 5475–5482.

Colbeck, S.C., 1987. A review of the metamorphism and classification of seasonal snow cover crystals. Avalanche Formation, Movement and Effects, vol. 162. IAHS Publication, Wallingford, Oxon, UK, pp. 1–34.

Edens, M.Q., Brown, R.L., 1991. Changes in microstructure of snow under large deformations. J. Glaciol. 37, 193–202.

Edens, M.Q., Brown, R.L., 1995. Measurements of microstructure of snow from surface sections. Def. Sci. J. 45, 107–116.

Fierz, C., Baunach, T., 2000. Quantifying grain shape changes in snow subjected to large temperature gradients. Ann. Glaciol. 31, 439–444.

Fierz, C., Lehning, M., 2001. Assessment of the microstructure-based snow-cover model SNOWPACK: thermal and mechanical properties. Cold Reg. Sci. Technol. 33, 123–131.

Fukuzawa, T., Akitaya, E., 1993. Depth-hoar crystal growth in the surface layer under high temperature gradient. Ann. Glaciol. 18, 39–45.

Giddings, J.C., LaChapelle, E., 1962. The formation rate of depth hoar. J. Geophys. Res. 67 (6), 2377–2383.

Gubler, H., 1985. Model for dry snow metamorphism by interparticle vapour flux. J. Geophys. Res. 90 (C8), 8081–8092.

Kojima, K., 1975. A field experiment on the rate of densification. Proceedings of the Grindelwald Symposium, vol. 114. IAHS Publication, Wallingford, Oxon, UK, pp. 298–308.

Lehning, M., Bartelt, P., Brown, R.L., Russi, T., Stöckli, U., Zimmerli, M., 1999. Snowpack model calculations for avalanche

warning based upon a new network of weather and snow stations. Cold Reg. Sci. Technol. 30, 145–157.

Lehning, M., Doorschot, J., Raderschall, N., Bartelt, P., 2000a. Combining snow drift and SNOWPACK models to estimate snow loading in avalanche slopes. In: Hjorth-Hansen, E., Holand, I., Loset, S., Norem, H. (Eds.), Snow Engineering. A.A. Balkema, Rotterdam, pp. 113–122.

Lehning, M., Doorschot, J., Bartelt, P., 2000b. A snow drift index based on SNOWPACK model calculations. Ann. Glaciol. 31, 382–386.

Lehning, M., Bartelt, P.B., Brown, R.L., Fierz, C., Satyawali, P., this issue. A physical SNOWPACK model for avalanche warning: Part III. Meteorological forcing, thin layer formation and evaluation. Cold Reg. Sci. Technol.

Mahajan, P., Brown, R.L., 1993. A microstructure-based constitutive law for snow. Ann. Glaciol. 18, 287–294.

Marbouty, B., 1980. An experimental study of temperature gradient metamorphism. J. Glaciol. 26, 303–312.

Sato, A., Adams, E.E., Brown, R.L., 1994. Effect of microstructure on heat and vapor transport in snow composed of uniform ice spheres. Proceedings of the International Snow Science Workshop, Snowbird, Utah. International Snow Science Workshop, Snowbird, Utah, pp. 176–184.

Shapiro, L.H., Johnson, J.B., Sturm, M., Blaisdell, G.L., 1997. Snow mechanics, review of the state of knowledge and applications. CRREL report 97-3, US Army Corps of Engineers, Hanover, 35 pp.

Sinha, N., 1978. Rheology of columnar-grained ice. Exp. Mech. 18 (79), 464–470.

Sturm, M., Benson, C.S., 1997. Vapor transport, grain growth and depth-hoar development in the subarctic snow. J. Glaciol. 43 (143), 42–59.